IEEE Access
Multidisciplinary ⋮ Rapid Review ⋮ Open Access Journal

Received March 22, 2020, accepted April 2, 2020, date of publication April 7, 2020, date of current version April 23, 2020.

Digital Object Identifier 10.1109/ACCESS.2020.2986384

Comparative Study of Novel Doubly-Fed Linear Switched Flux Permanent Magnet Machines With Different Primary Structures

LIJIAN WU, (Senior Member, IEEE), LIU ZHANG, JIABEI ZHU, QINFEN LU, (Senior Member, IEEE), AND YOUTONG FANG, (Senior Member, IEEE)
College of Electrical Engineering, Zhejiang University, Hangzhou 310027, China

Corresponding author: Liu Zhang (liuzhang@zju.edu.cn)

This work was supported in part by the National Natural Science Foundation of China under Grant 51977191, Grant 51677169, Grant 51637009, and Grant 51827810, and in part by the National Key Research and Development Program of China under Grant 2018YFB1501304.

ABSTRACT To enhance the thrust force density and move a part of copper loss from the primary to the secondary of linear switched flux permanent magnet machines (LSFPMMs), this paper proposes a novel kind of doubly-fed LSFPMMs (DFLSFPMMs) by adding another set of armature winding on the secondary of LSFPMMs. The design and working principles of the new winding are analyzed first. It is found that the optimal coil pitch depends on the primary structure. Then, the parameters of DFLSFPMMs with U-core, C-core, E-core, and multi-tooth primary structures are globally optimized, and their electromagnetic performances are investigated by 2D finite element method. The result shows that the average thrust force of U-core DFLSFPMM is 30% higher than that of conventional LSFPMM counterpart, and it is also 23%-29% higher than those of DFLSFPMMs with other three primary structures. Besides, the U-core machine with tubular structure is analyzed for the potential application of electromagnetic shock absorbers, which shows the U-core DFLSFPMM has 10% higher peak-to-peak damping force than linear spoken-type PM machine. Finally, a prototype of U-core DFLSFPMM is manufactured and tested to validate the analysis.

INDEX TERMS Doubly-fed, linear machine, permanent magnet, primary structure, switched flux.

I. INTRODUCTION

By employing high performance permanent magnets (PMs), PM machines have attracted more and more attention due to high power density and efficiency [1], [2]. Meanwhile, a series of stator PM machines, namely, switched flux PM machines (SFPMMs), doubly salient PM machines (DSPMMs), and flux reversal PM machines (FRPMMs), were proposed and developed in recent decades [3]–[5]. It was reported that DSPMMs, of which the PMs are inserted in the stator back iron and number of stator poles between adjacent PMs is equal to the phase number, suffer unbalanced phase flux linkages and back-EMFs [6], while FRPMMs with PMs on the surface of stator teeth have relatively larger effective air gap length and higher risk of irreversible demagnetization [7]. As for SFPMMs, besides their balanced three phase and low demagnetization risk, the flux-focusing structures make them exhibit much higher power density than DSPMMs and FRPMMs [8], [9]. Therefore, much more research works about SFPMMs were carried out.

The combination of U-core stator and salient rotor is one of the most common structures for SFPMMs [10]. In such structure, each PM with circumferential magnetization is sandwiched between two U-shaped stator core segments, and the stator pole is defined as one PM with two adjacent stator teeth. The concentrated windings are wound over the stator poles while neither PMs nor windings are on the rotor. Moreover, an E-core stator was proposed by replacing every alternative stator pole with stator tooth [11]. After replacement, the stator teeth at the middle of adjacent stator poles physically and magnetically separate the adjacent coils, enhancing the fault-tolerant capability of the machine. Furthermore, the middle stator teeth in E-core stator can be removed to increase the slot area, which is designated as the C-core stator [12]. It should be mentioned that the C-core stator can also be regarded as a U-core stator but with much

The associate editor coordinating the review of this manuscript and approving it for publication was Giovanni Angiulli.

larger slot opening. In addition, based on the C-core stator, a multi-tooth stator was obtained by splitting the stator tooth-tips into several small teeth, which helps to increase the rotor pole number and electric frequency [13].

On the other hand, linear machines have become a hot spot since they directly transfer the electric energy to the linear motion mechanical energy [14], which are favorable for applications of electromagnetic launch system and railway transportation [15], [16]. The structures of rotary SFPMMs mentioned before can also be employed in linear SFPMMs (LSFPMMs). In [17] and [18], the investigations of LSFPMMs with U-core primary showed this kind of machines have higher thrust force density when the secondary pole number is close to the primary pole number. In [19], the analysis of LSFPMMs with C-core primary and E-core primary proved that the 6/13 and 6/11 primary/secondary-pole combinations are better for C-core and E-core LSFPMMs, respectively. In [20] and [21], the studies of LSFPMMs with multi-tooth primary concluded that the secondary pole number about triple the primary pole number is more preferred in such machines.

However, compared with U-core LSFPMMs, although C-core, E-core, and multi-tooth LSFPMMs exhibit some superior characteristics, the thrust force density is not improved significantly. Meanwhile, since the PMs are surrounded by the iron core and armature winding, it is not easy to manage the PM temperature in LSFPMMs. A partitioned primary structure was proposed to solve these problems [22], [23]. In this structure, the primary is separated into two parts and placed at two sides of the secondary. The PMs are on the one part of primary and the armature winding is on the other part, while the secondary only consists of iron pieces. It has been evidenced that LSFPMMs with partitioned primary have higher thrust force density than U-core and E-core LSFPMMs [24], [25]. Nevertheless, the complicated structures of partitioned primary LSFPMMs increase the manufacturing inaccuracy, and hence reduce the performance of prototype machine [23], [24].

For conventional LSFPMMs, the armature windings are wound on primary poles since the flux through primary poles varies with the mover motion, while this variation also exists in secondary poles. Thereby, it is possible to produce power by injecting AC current into windings wound on secondary poles, enhancing the thrust force density as well as moving a part of copper loss from the primary to the secondary.

In this paper, four flat doubly-fed LSFPMMs (DFLSFPMMs) are proposed by adding another set of armature winding on the secondary of the U-core, C-core, E-core, and multi-tooth LSFPMMs, respectively. In Section II, the topologies and operation principles of these DFLSFPMMs are introduced. Then, the electromagnetic performances of DFLSFPMMs and their LSFPMMs counterparts are compared in Section III. Afterwards, the potential application of DFLSFPMM is analyzed in Section IV. Finally, a prototype machine is manufactured to validate the analysis results.

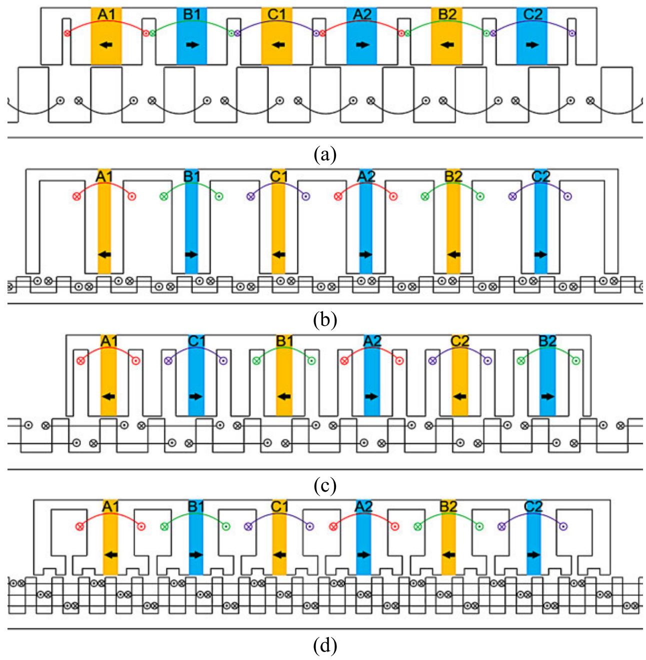

FIGURE 1. Topologies of DFLSFPMMs. (a) U-core. (b) C-core. (c) E-core. (d) Multi-tooth.

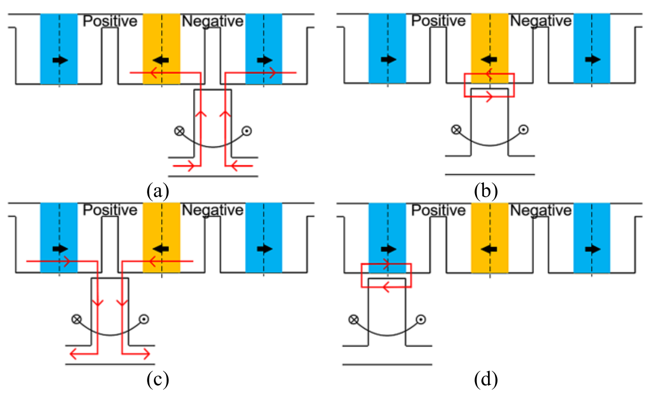

FIGURE 2. Flux path variation with mover position in U-core DFLSFPMM. (a) 0 elec. degree. (b) 90 elec. degree. (c) 180 elec. degree. (d) 270 elec. degree.

II. MACHINE TOPOLOGY AND OPERATION PRINCIPLE

The topologies of U-core DFLSFPMM with 6/7 primary/secondary-pole, C-core DFLSFPMM with 6/13 primary/secondary-pole, E-core DFLSFPMM with 6/11 primary/secondary-pole, and multi-tooth DFLSFPMM with 6/19 primary/secondary-pole are shown in Fig. 1. Obviously, the DFLSFPMMs have similar structures with the LSFPMMs counterparts, except the armature windings on the secondary. Hence, the design and working principles of primary winding in the DFLSFPMMs are similar to those in the LSFPMMs.

As for the secondary winding, its working principle can be analyzed by a simplified model, as shown in Fig. 2. The primary can be divided into two parts in terms of PM magnetization direction, i.e. positive part and negative part, and they are alternately distributed on the primary. When the

TABLE 1. Fixed parameters of LSFPMMS and DFLSFPMMS.

Parameters	Unit	LSFPMM				DFLSFPMM			
		U-core	C-core	E-core	Multi-tooth	U-core	C-core	E-core	Multi-tooth
Machine height, h	mm	50							
Stack length, l	mm	50							
Air gap length, g	mm	1							
PM remanence, B_r	T	1.2							
Relative PM permeability, μ_r	-	1.05							
Speed, v	m/s	0.96							
Total copper loss within active length, P_{cu}	W	40							
Rated AC current, I_{rms}	Arms	3.54							
Packing factor, p_f	-	0.4							
Number of active primary poles, N_p	-	6							
Primary pole pitch, l_p	mm	32							
Number of active secondary poles, N_s	-	7	13	11	19	7	13	11	19
Secondary pole pitch, l_s	mm	27.4	14.8	17.5	10.1	27.4	14.8	17.5	10.1

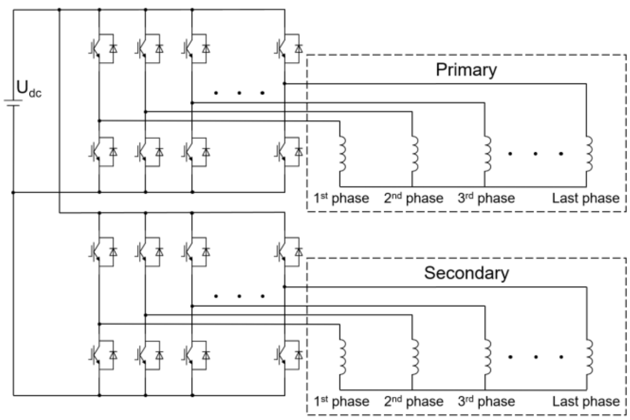

FIGURE 3. Power supply circuit of DFLSFPMM.

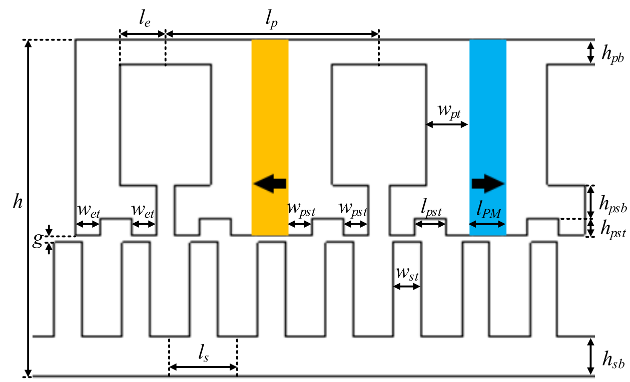

FIGURE 4. Illustration of geometric parameters.

secondary pole is between two adjacent PMs [e.g. in negative part shown in Fig. 2(a)], the coil wound on this pole has negative flux linkage. As the mover moves to a position where the secondary pole aligns the PM, the flux is short circuited and thus the coil flux linkage is zero. Then, the secondary pole is in the next primary part [e.g. positive part shown in Fig. 2(c)], where the flux direction becomes opposite and the coil has positive flux linkage. After that, the secondary pole aligns the next PM and the coil flux linkage is zero again. Finally, the secondary pole is in the next negative part, which is the same condition as that shown in Fig. 2(a). Consequently, the secondary coil can obtain bipolar flux linkage with the mover motion.

Meanwhile, the coil pitch should be optimized to achieve higher coil pitch factor. The secondary coil pitch factor K_{ps} of DFLSFPMMs can be calculated by (1), where N_p is the number of primary poles, N_s is the number of secondary poles, and n_s is the secondary coil pitch (i.e. number of secondary poles one coil spans). It indicates that to achieve high K_{ps}, the secondary coil pitch should be close to the secondary to primary pole number ratio. Therefore, for the U-core DFLSFPMM which has comparable secondary and primary pole numbers, the non-overlapping secondary winding is more desirable, while the overlapping secondary windings with $n_s = 2$ are more suitable for the C-core and E-core DFLSFPMMs since their secondary pole numbers are roughly twice the primary pole numbers. As for the multi-tooth DFLSFPMM, the overlapping secondary winding with $n_s = 3$ is better.

$$K_{ps} = \cos\left[\frac{\pi}{2}\left(\frac{N_p n_s}{N_s} - 1\right)\right] \quad (1)$$

Besides, due to the prime number of secondary poles, the secondary phase number is equal to the secondary pole number in each DFLSFPMM. Thus, the secondary winding factors of the U-core, C-core, E-core, and multi-tooth DFLSFPMMs are 0.975, 0.993, 0.990, and 0.997, respectively. The power supply circuit of DFLSFPMM is shown in Fig. 3. Because of two armature windings, each machine needs two multi-phase full-bridge converters.

III. ELECTROMAGNETIC PERFORMANCE COMPARISON

By using the parametric sweep and 2D finite element (FE) methods, these four DFLSFPMMs and their conventional counterparts without secondary winding are globally optimized. The cross-sections of optimized DFLSFPMMs are shown in Fig. 1 while the parameters are listed in TABLE 1 and TABLE 2. Meanwhile, Fig. 4 illustrates the key geometric parameters of the machines. During the optimization, the

TABLE 2. Optimized parameters of LSFPMMS and DFLSFPMMS.

Parameters	Unit	LSFPMM				DFLSFPMM			
		U-core	C-core	E-core	Multi-tooth	U-core	C-core	E-core	Multi-tooth
Split ratio, λ	-	0.26	0.22	0.26	0.22	0.56	0.22	0.40	0.42
PM length, l_{PM}	mm	5.5	3.8	4.0	3.3	11.0	4.1	5.2	4.5
Primary tooth width, w_{pt}	mm	7.3	4.8	5.0	7.6	8.0	5.0	4.8	6.7
Primary back iron height, h_{pb}	mm	4.9	4.2	5.7	5.7	4.3	4.1	5.4	3.8
Turns per coil of primary windings, N_{cp}	-	122	160	134	121	26	149	77	69
Primary copper loss, P_{cup}	W	40	40	40	40	8	36	22	18
Secondary tooth width, w_{st}	mm	10.3	5.1	6.0	3.5	11.6	5.3	6.2	4.1
Secondary back iron height, h_{sb}	mm	5.5	4.6	6.4	6.1	5.9	4.0	6.5	5.9
Turns per coil of secondary windings, N_{cs}	-	-	-	-	-	98	10	36	24
Secondary copper loss, P_{cus}	W	0	0	0	0	32	4	18	22
End tooth width, w_{et}	mm	6.3	4.6	2.0	3.8	8.0	5.0	2.8	3.8
End back iron length, l_e	mm	5.5	9.0	0	6.6	0.5	7.5	0	6.5
Primary middle tooth width, w_{pmt}	mm	-	-	4.0	-	-	-	6.8	-
Primary small tooth width, w_{pst}	mm	-	-	-	3.8	-	-	-	3.8
Primary small tooth height, h_{pst}	mm	-	-	-	2.7	-	-	-	2.5
Primary small tooth distance, l_{pst}	mm	-	-	-	5.1	-	-	-	4.6
Primary small back iron height, h_{psb}	mm	-	-	-	4.4	-	-	-	4.9

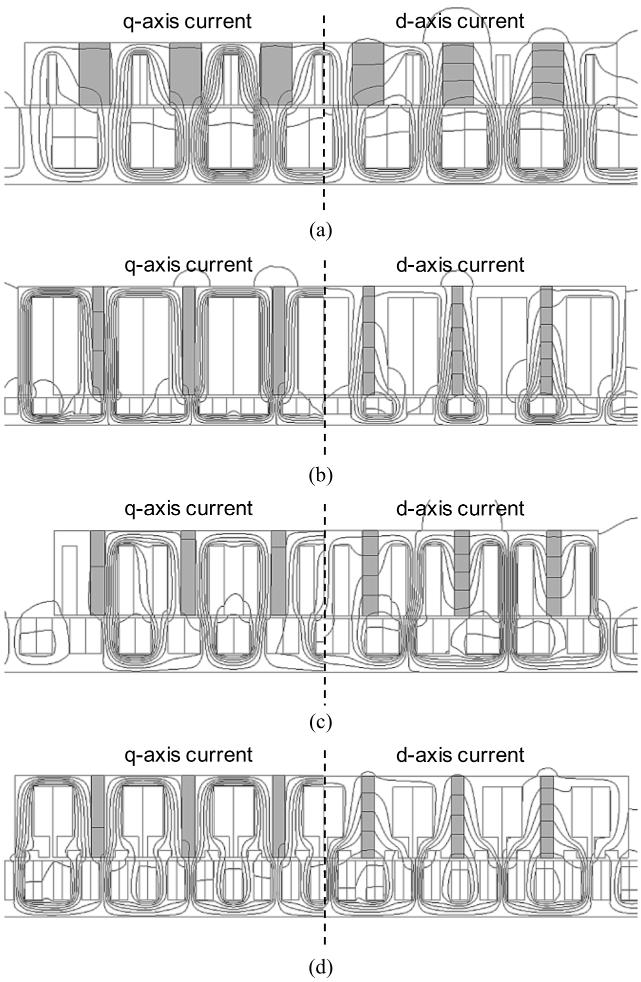

FIGURE 5. Magnetic field distributions excited by secondary winding in DFLSFPMMs. (a) U-core. (b) C-core. (c) E-core. (d) Multi-tooth.

primary end teeth are employed to reduce the longitudinal end effect and the primary middle teeth in the E-core LSFPMM

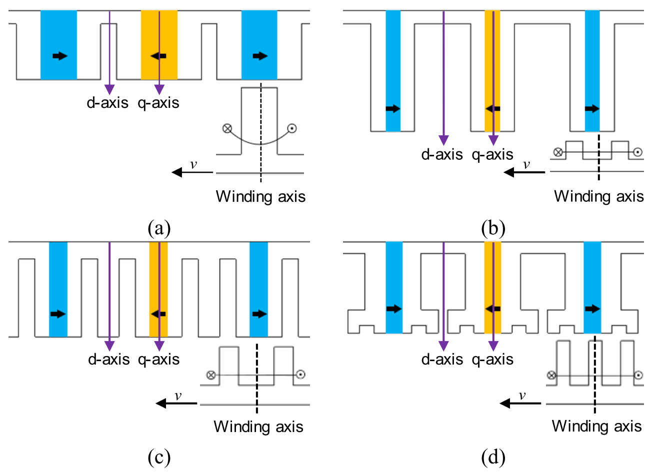

FIGURE 6. D- and q-axes of secondary in DFLSFPMMs. (a) U-core. (b) C-core. (c) E-core. (d) Multi-tooth.

are remained for the fault tolerant capability, while the other parameters are optimized for the maximum average thrust force under the fundamental AC current injection. It should be noticed that the electric frequency for primary f_{ep} and secondary f_{es} in the DFLSFPMMs are different, which can be expressed by (2) and (3), respectively.

$$f_{ep} = \frac{v}{l_s} \tag{2}$$

$$f_{es} = \frac{v}{2l_p} \tag{3}$$

Besides, to achieve similar thermal conditions, the copper loss only produced in the secondary with the same length of primary without end teeth is considered as the secondary copper loss. Moreover, because the total copper loss within active length, rms value of rated AC current, and packing factor are fixed, the number of turns per coil should be varied with the slot area, as shown in (4) and (5). The A_{sp} and A_{ss} stand for the primary and secondary slot areas for one coil side respectively, l_{cp} and l_{cs} stand for the one-turn-length of

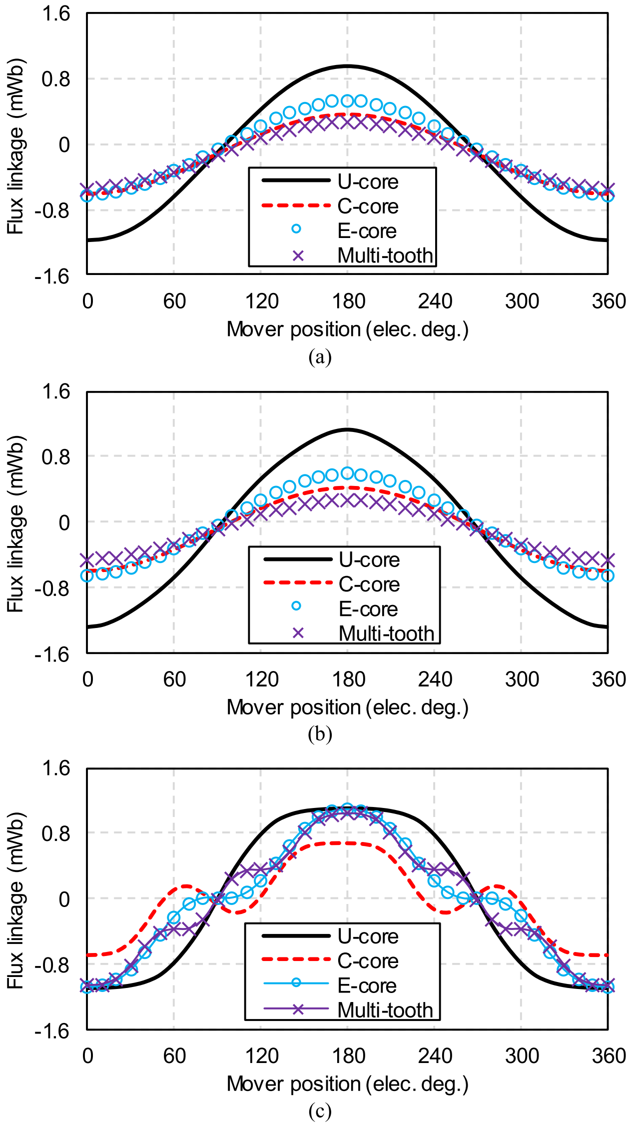

FIGURE 7. Waveforms of open-circuit phase flux linkage with $N_{cp} = N_{cs} = 1$. (a) LSFPMMs. (b) Primary of DFLSFPMMs. (c) Secondary of DFLSFPMMs.

primary and secondary coils respectively. In addition, the split ratio is defined in (6), where h_s is the secondary height.

$$N_{cp} = \sqrt{\frac{P_{cup}P_f A_{sp}}{N_p I_{rms}^2 \rho l_{cp}}} \tag{4}$$

$$N_{cs} = \sqrt{\frac{P_{cus}P_f A_{ss}}{N_s I_{rms}^2 \rho l_{cs}}} \tag{5}$$

$$\lambda = \frac{h_s + g}{h} \tag{6}$$

A. SECONDARY ARMATURE REACTION FIELD DISTRIBUTION

Since the open-circuit and primary armature reaction field distributions have been widely analyzed [10]–[13], this sub-

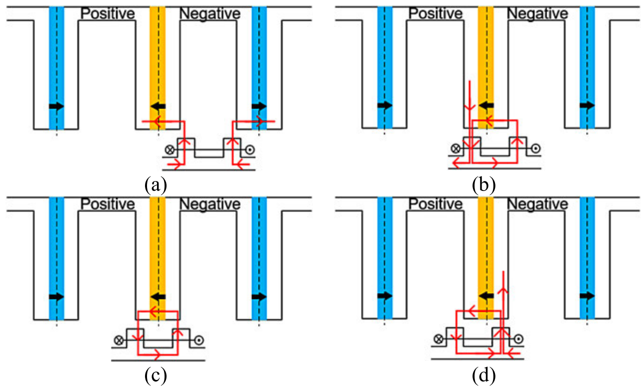

FIGURE 8. Flux path variation with mover position in C-core DFLSFPMM. (a) 0 elec. degree. (b) 70 elec. degree. (c) 90 elec. degree. (d) 110 elec. degree.

section only investigates the secondary armature reaction. In the conventional LSFPMMs, the primary armature reaction field, whether excited by q-axis current or d-axis current, only has a little flux passing through the PMs [3], thus the LSFPMMs have the merit of low demagnetization risk. However, as shown in Fig. 5, much more flux penetrates the PMs when the field is excited by the d-axis current of secondary winding. The d- and q-axes of secondary in DFLSFPMMs are illustrated in Fig. 6. When the winding axis aligns the d-axis, the winding has the maximum positive flux linkage, and the q-axis leads d-axis by 90 elec. deg. As can be noticed, if the DFLSFPMMs are designed to operate under the flux-weakening condition, it is more necessary to check the machine capability of demagnetization withstanding, especially for the C-core, E-core, and multi-tooth DFLSFPMMs, whose PMs are relatively thinner.

B. OPEN-CIRCUIT FLUX LINKAGE

The waveforms of open-circuit phase flux linkage with one turn per coil are shown in Fig. 7. Regardless of primary structures, all the LSFPMMs and DFLSFPMMs have sinusoidal primary phase flux linkages. On the contrary, the waveforms of secondary phase flux linkages in four DFLSFPMMs are obviously different. For the U-core DFLSFPMM, it has trapezoidal secondary flux linkage, which is consistent with the operation principle analysis. As for the C-core DFLSFPMM, more fluctuations are observed in its waveforms. This phenomenon can be analyzed as follows. When two secondary poles wound with the same coil are in the same negative part shown in Fig. 8(a), the coil has negative flux linkage. Then, as one of the secondary pole moves into the positive part shown in Fig. 8(b), the flux directions in two poles are opposite. Since the overlapping area between primary and secondary teeth in the positive part is larger than that in the negative part, the coil flux linkage becomes positive. After that, as the mover continue moving, the air gap permeance reduces in the positive part but increases in the negative part, thus the coil flux linkage reduces to zero [Fig. 8(c)] and even becomes negative again [Fig. 8(d)]. Finally, when both of the

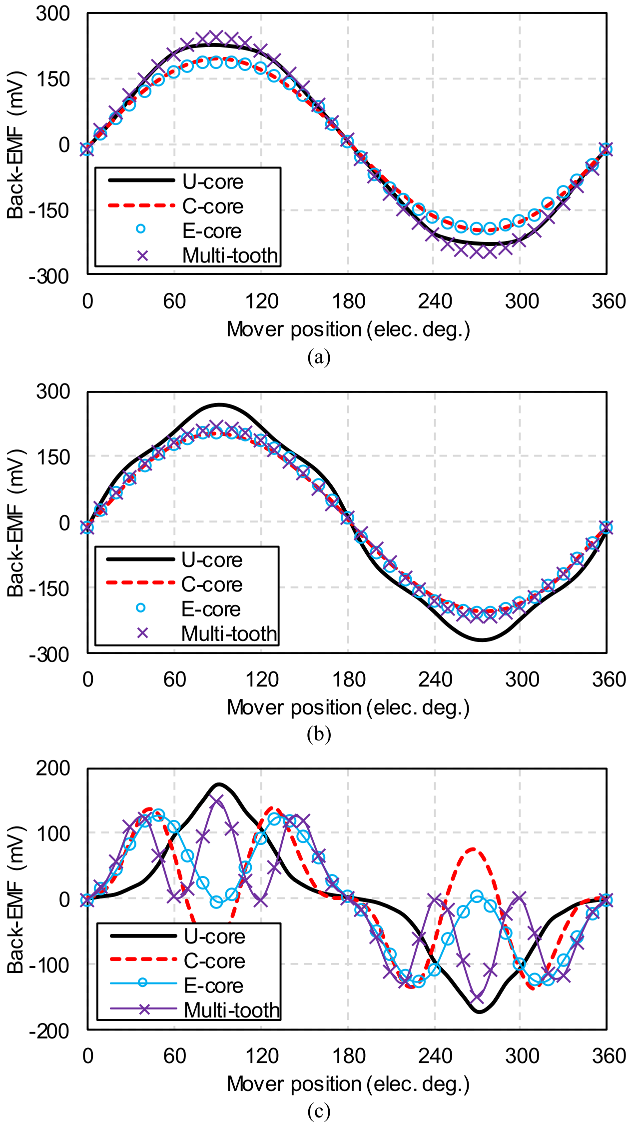

FIGURE 9. **Waveforms of open-circuit phase back-EMF with $N_{cp} = N_{cs} = 1$. (a) LSFPMMs. (b) Primary of DFLSFPMMs. (c) Secondary of DFLSFPMMs.**

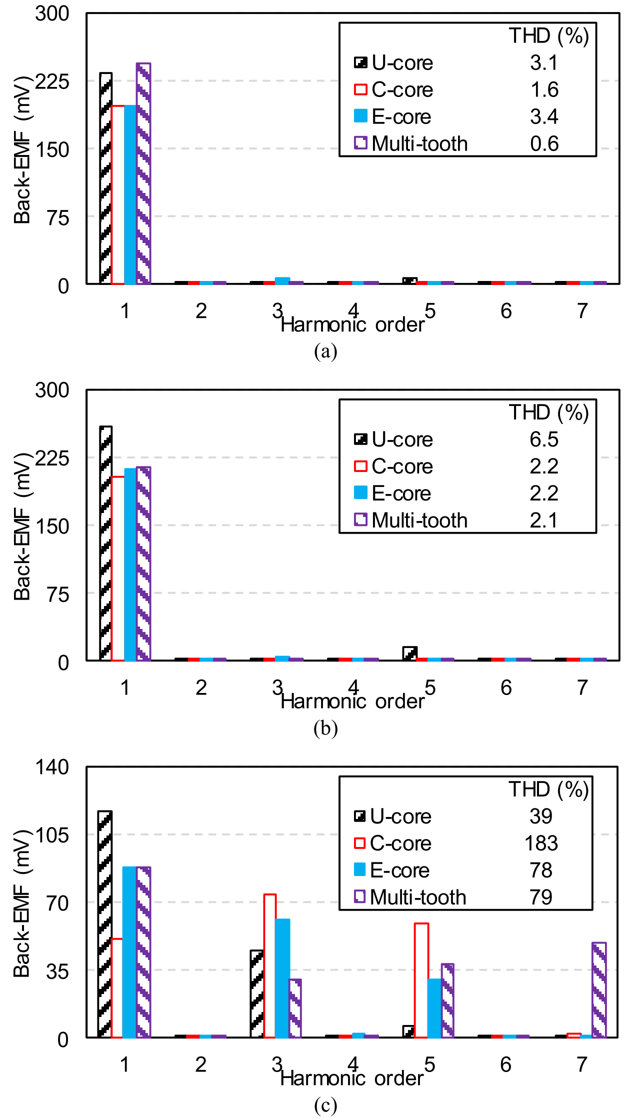

FIGURE 10. **Spectra of open-circuit phase back-EMF with $N_{cp} = N_{cs} = 1$. (a) LSFPMMs. (b) Primary of DFLSFPMMs. (c) Secondary of DFLSFPMMs.**

secondary poles are in the positive part, the coil flux linkage changes to positive once more. The similar phenomena also exist in the E-core and multi-tooth DFLSFPMMs, while the fluctuations are not as apparent as those in the C-core DFLSFPMM due to the primary middle teeth and primary small teeth.

C. OPEN-CIRCUIT BACK-EMF

Fig. 9 and Fig. 10 show the waveforms and spectra of open-circuit phase back-EMF, respectively. It can be found that the total harmonic distortions (THDs) of the primary phase back-EMF in these machines are relatively small, while a large number of harmonic components exist in the secondary phase back-EMF of DFLSFPMMs. Comparatively, the U-core DFLSFPMM has the largest fundamental component of secondary phase back-EMF, thus it has the largest split ratio among four DFLSFPMMs. By contrast, the smallest fundamental component in the C-core DFLSFPMM makes its optimized parameters similar to those of the C-core LSFPMM.

D. DETENT FORCE

Fig. 11 compares the detent force of these machines. In this paper, the machines have short primary structures. Thus, the period of detent force is equal to the electric period of primary. As can be observed, the U-core machines have large 6^{th} harmonic components in the detent force, which are mainly caused by the slot-effect. For other machines, the components caused by the end-effect dominate the detent force. On the other hand, the U-core machines exhibit much larger detent force than the others, while it can be mitigated by reducing the slot-effect (e.g. skew the secondary poles).

TABLE 3. Force performance of LSFPMMS and DFLSFPMMS.

Items	Unit	LSFPMM				DFLSFPMM			
		U-core	C-core	E-core	Multi-tooth	U-core	C-core	E-core	Multi-tooth
Average thrust force	N	197.5	199.7	176.2	180.1	256.0	208.5	202.1	199.2
Thrust force per PM volume	N/cm^3	3.24	4.49	3.97	4.67	3.53	4.35	4.32	5.09
Thrust force ripple	%	37.5	21.1	14.8	15.4	22.9	27.0	9.2	14.6

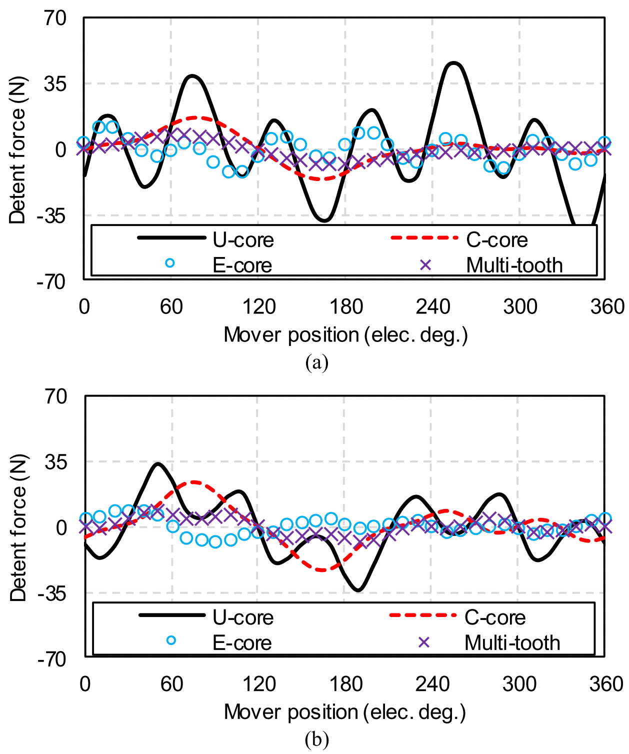

FIGURE 11. Detent force waveforms. (a) LSFPMMs. (b) DFLSFPMMs.

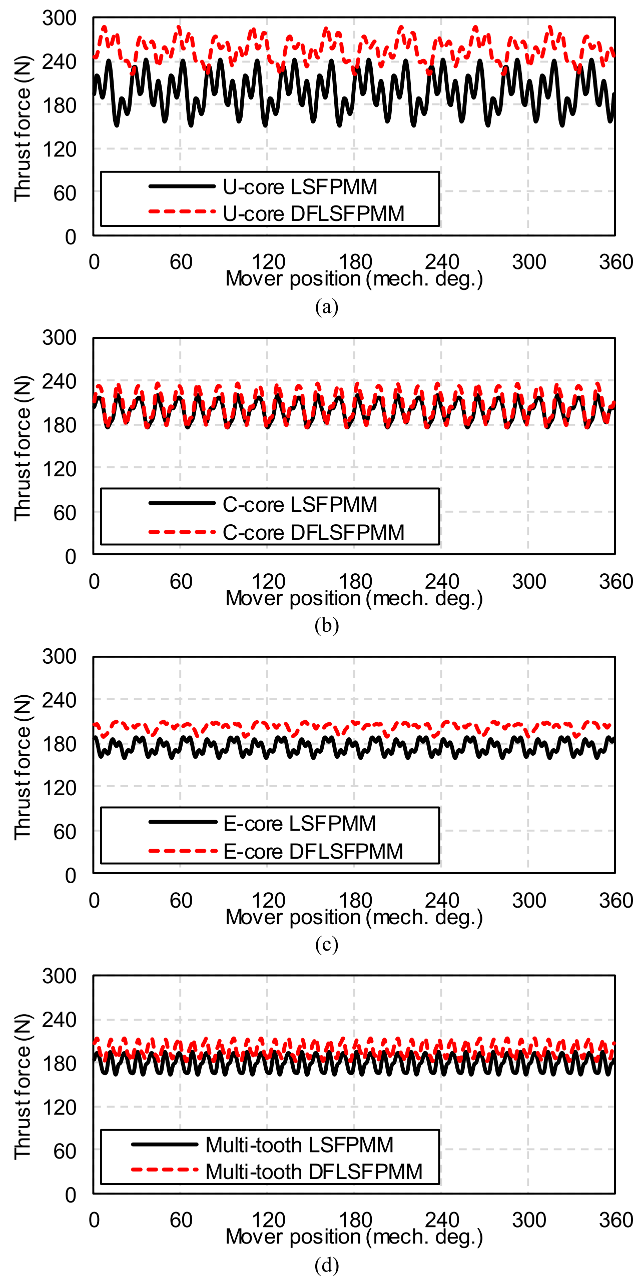

FIGURE 12. Thrust force waveforms. (a) U-core LSFPMM and DFLSFPMM. (b) C-core LSFPMM and DFLSFPMM. (c) E-core LSFPMM and DFLSFPMM. (d) Multi-tooth LSFPMM and DFLSFPMM.

E. THRUST FORCE

The thrust force performances of LSFPMMs and DFLSFPMMs are compared in Fig. 12 and TABLE 3. It shows that the U-core, C-core, E-core, and multi-tooth DFLSFPMMs exhibit 30%, 4%, 15%, and 11% higher average thrust force than their LSFPMMs counterparts, respectively. On the other hand, the U-core LSFPMM is sometimes not the best one among the LSFPMMs since the other three machines can achieve comparable average thrust force with much higher PM usage efficiency (i.e. thrust force per PM volume). However, although the PM usage efficiency of the U-core DFLSFPMM is still relatively low among the DFLSPMMs, its average thrust force is much higher than the others. As for the thrust force ripple, which is defined as the ratio of peak-to-peak force to average force, it is 22.9% in the U-core DFLSFPMM, smaller than those of the U-core LSFPMM and C-core DFLSFPMM, but larger than those of the E-core and multi-tooth DFLSFPMMs.

Fig. 13 shows the variation of average thrust force with primary and secondary current angles in the DFLSFPMM. The current angle is defined as the phase difference between back-EMF and current. For each DFLSFPMM, the maximum average thrust force is achieved when both primary and secondary current angles are around 0 elec. deg. It indicates that

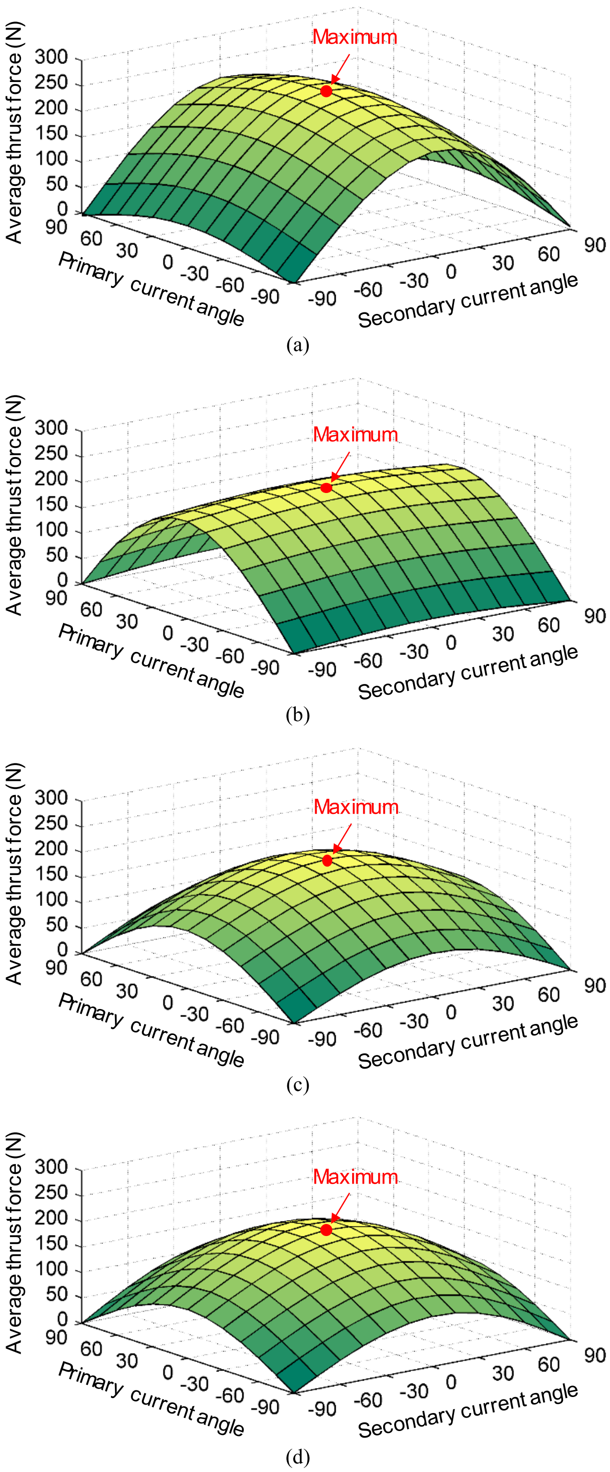

FIGURE 13. Thrust force versus primary and secondary current angles in DFLSFPMM, the unit of current angle is elec. deg. (a) U-core. (b) C-core. (c) E-core. (d) Multi-tooth.

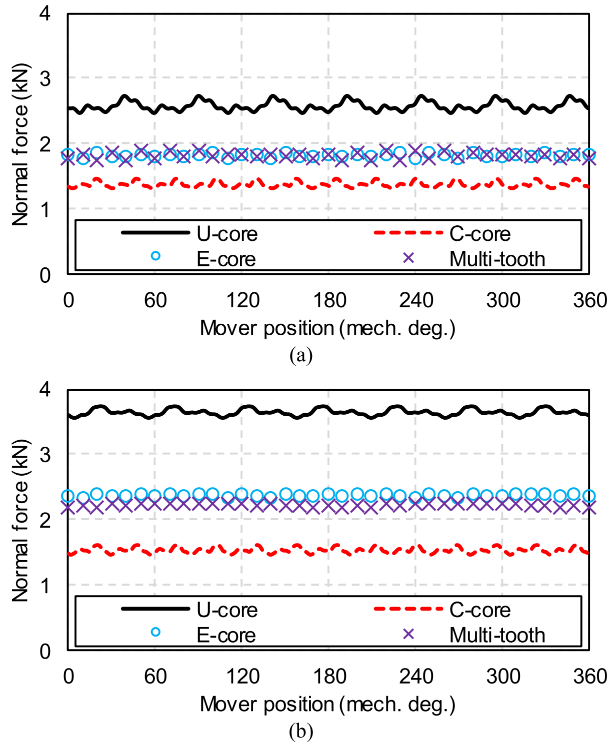

FIGURE 14. Normal force waveforms. (a) LSFPMMs. (b) DFLSFPMMs.

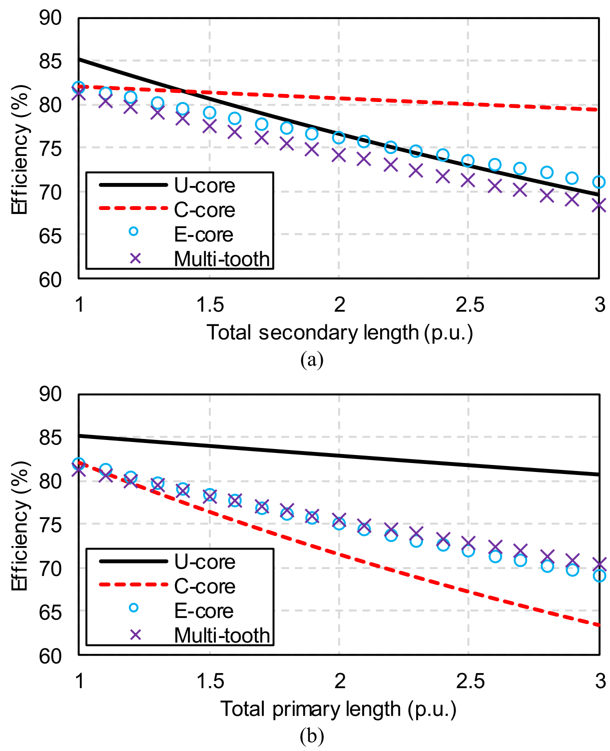

FIGURE 15. Efficiencies of DFLSFPMMs, the base value of total secondary/primary length is the active machine length. (a) Short primary structure. (b) Short secondary structure.

both armature windings in the DFLSFPMMs can be operated with the zero d-axis current control strategy.

F. NORMAL FORCE

Fig. 14 compares the normal force of these machines. The DFLSFPMMs have larger normal force than their LSFPMM counterparts due to the increased PM usage. Especially, the normal force of U-core DFLSFPMM is much higher than the others, while it can be reduced when the machine has double sided or tubular structures.

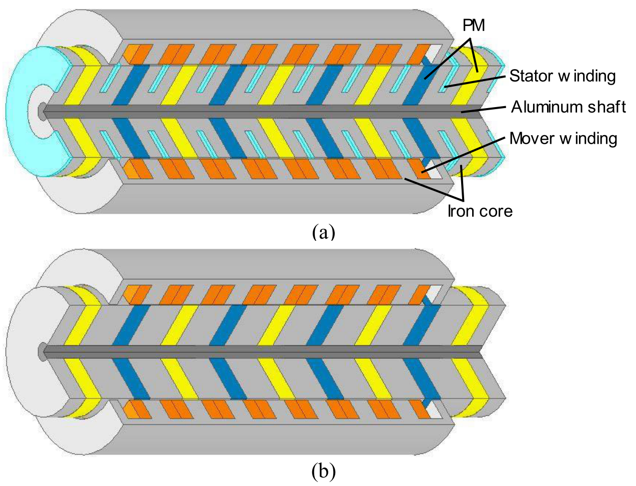

FIGURE 16. Tubular machine structures. (a) U-core DFLSFPMM. (b) LSTPMM.

TABLE 4. Key data of tubular machines.

Items	Value	
	DFLSFPMM	LSTPMM
Outer diameter (mm)	110	
Shaft diameter (mm)	10	
Air gap length (mm)	1	
Mover pole pitch (mm)	27.4	
Stator pole pitch (mm)	32	
Number of mover poles	7	
Number of stator poles	9	
Stator outer diameter (mm)	70	70
Stator tooth width (mm)	8.6	-
Stator back iron height (mm)	9.7	-
PM thickness (mm)	10.4	10.4
Stator turns per coil	44	-
Mover tooth width (mm)	10.4	11.8
Mover back iron height (mm)	4.0	4.5
Mover turns per coil	126	132

G. EFFICIENCY

Taking the copper loss and core loss into account, the efficiencies of these machines are calculated. In LSFPMMs, the winding is only on the primary. Therefore, when short primary structure is employed, the efficiencies of LSFPMMs are not varied with the total secondary length. In this paper, the efficiencies of the U-core, C-core, E-core, and multi-tooth LSFPMMs are 82%, 81%, 79%, and 78%, respectively. On the contrary, the windings are wound on both primary and secondary poles in DFLSFPMMs. When the segment-powered method is not used, the copper loss increases with the total machine length, and thus reduce the efficiency. Fig. 15 shows the variations of efficiency with total machine length in short primary and short secondary structures. For each structure, the active machine length is equal to that shown in TABLE 1. Since the U-core DFLSFPMM has large secondary copper loss within the active length, its efficiency decreases significantly with the total secondary length when such machine has the short primary structure. On the other hand, with the short secondary structure, the efficiency of U-core DFLSFPMM is still over 80% when the primary is three times as long as the secondary.

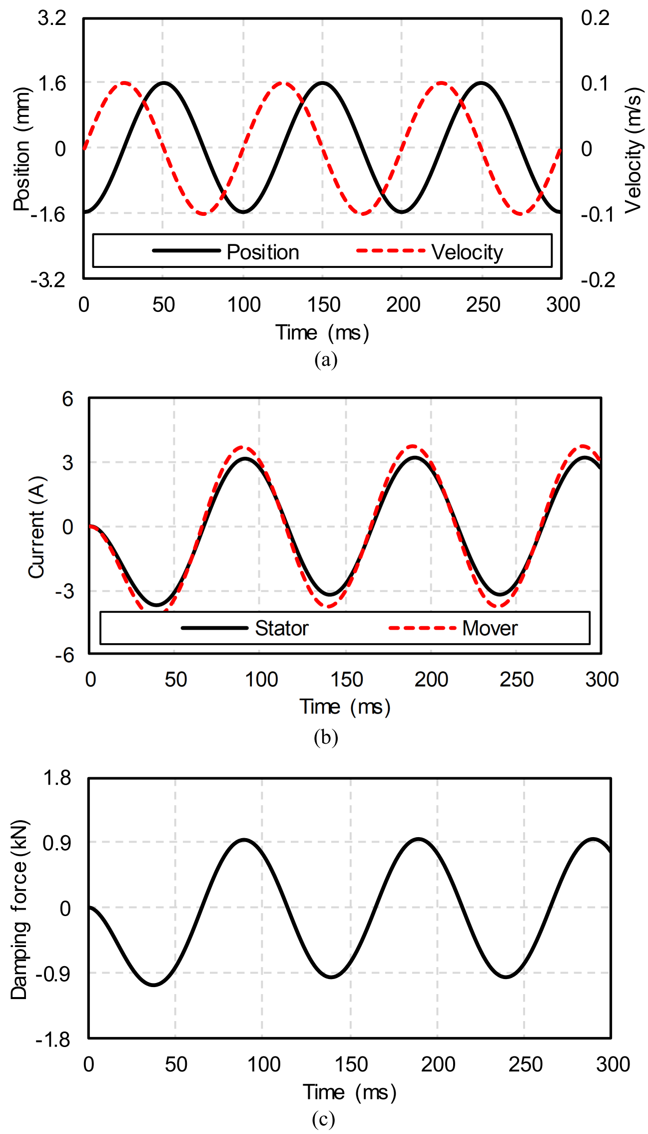

FIGURE 17. Performances of U-core DFLSFPMM with 10 Hz, 0.1m/s peak velocity vibration. (a) Mover position and velocity. (b) Current of the phase having the maximum magnitudes. (c) Damping force.

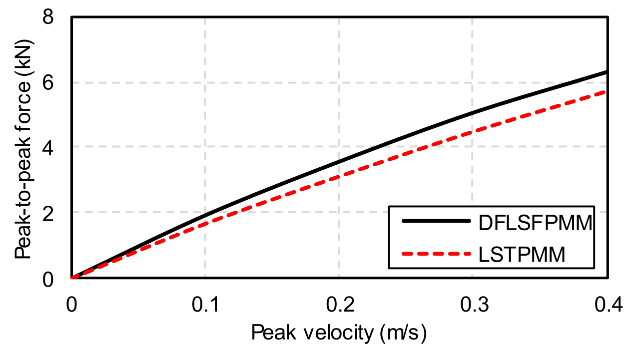

FIGURE 18. Peak-to-peak damping force versus peak velocity of vibration.

IV. APPLICATION

For long stroke applications, the LSFPMMs are desirable choices since both PM and winding can be assembled on the short mover. However, due to the windings on both mover

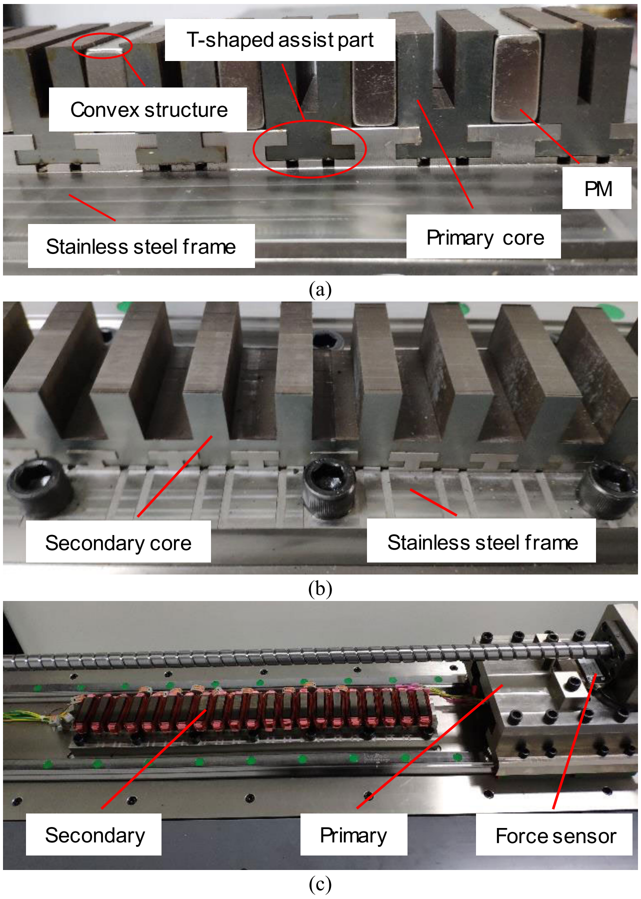

FIGURE 19. Prototype machine photos. (a) Primary core and PMs. (b) Secondary core. (c) Test rig.

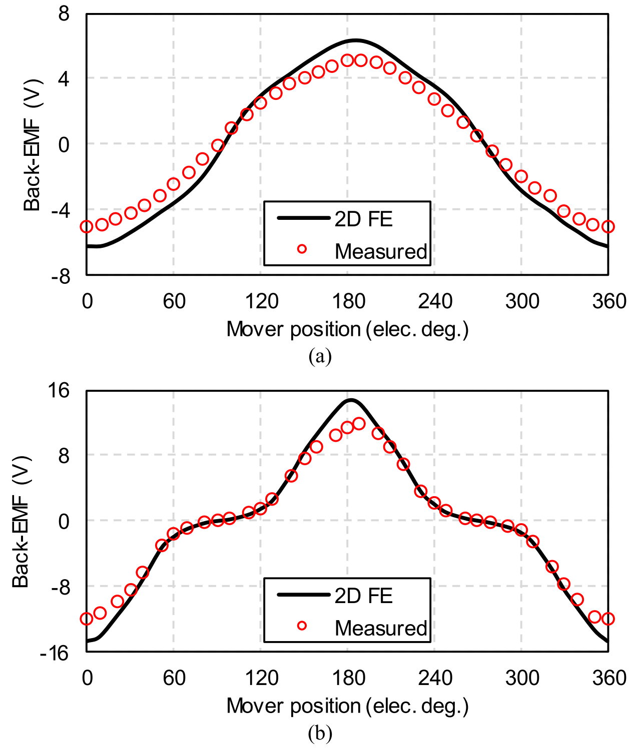

FIGURE 20. 2D FE predicted and measured phase back-EMFs. (a) Primary. (b) Secondary.

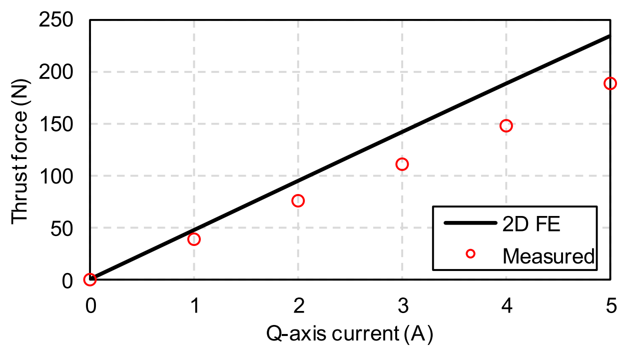

FIGURE 21. 2D FE predicted and measured force-current characteristics.

and stator, the DFLSFPMMs are less competitive for such applications in terms of cost and efficiency. Similar with linear secondary PM machines, the DFLSFPMMs are more suitable for short stroke applications, e.g. machine tools and electromagnetic shock absorbers [26]-[28]. For flat DFLSFPMMs applied in machine tools, their performances can be deduced from Section III. Hence, in this section, a tubular U-core DFLSFPMM and a tubular linear spoken-type PM machine (LSTPMM) are analyzed and compared for the application of electromagnetic shock absorbers. The structures of two machines are shown in Fig. 16 while the main parameters are listed in TABLE 4. The PM usages of two machines are the same. Fig. 17 shows the performances of U-core DFLSFPMM when its mover is excited by a 10 Hz, 0.1 m/s peak velocity sinusoidal vibration and its windings are short circuited with star connection. Meanwhile, as compared in Fig. 18, the U-core DFLSFPMM can achieve >10% higher peak-to-peak damping force than LSTPMM when the peak velocity of vibration is between 0.1-0.4 m/s.

V. EXPERIMENTAL VALIDATION

The flat U-core DFLSFPMM is manufactured to validate the previous analysis, as shown in Fig. 19. For easy manufacturing, a convex structure is introduced next to the primary tooth-tips to help fix the PMs, and the PM height is reduced by 1 mm to fit such structure. Besides, a T-shaped assist part is added on both primary and secondary cores, which is used for assembling machine on the stainless steel frame.

The phase back-EMFs are measured when the ball screw as well as machine primary is driven by a servo motor. As compared in Fig. 20, in general, the back-EMF waveforms of FE prediction and measurement have a good agreement, while the magnitudes of measured results are 20% lower than the FE prediction. This is mainly caused by the transverse end effect, which is similar to conventional SFPMMs and LSFPMMs. The 2D FE predicted and measured force-current characteristics are shown in Fig. 21. In each case, the magnitudes of q-axis current injected in the primary and secondary windings are the same. During the measurement, the machine primary is fixed first, and then the winding current is injected by DC power supplies. The injected current is equal to q-axis current of the corresponding primary position. As can be seen, for each value of q-axis current, the measured thrust force is approximately 20% lower than the FE prediction, which is consistent with the back-EMF measurement. Overall, the measured results validate the previous 2D FE analysis.

VI. CONCLUSION

In this paper, four DFLSPMMs are proposed by adding secondary windings in the conventional LSFPMMs. The secondary coil pitch should be close to the ratio of secondary to primary pole number, thus the winding types of these DFLSFPMMs are different. The electromagnetic performance analysis shows that the U-core DFLSFPMM with concentrated secondary winding can achieve the highest average thrust force among these machines, while the C-core, E-core, and multi-tooth DFLSFPMMs with distributed secondary windings have much more harmonics in the secondary phase flux linkages and back-EMFs. Moreover, different with LSFPMMs, the DFLSFPMMs are more competitive for short stroke applications, such as the electromagnetic shock absorber. The dynamic performances and experiment under such applications are required in future investigations.

REFERENCES

[1] K. T. Chau, C. C. Chan, and C. Liu, "Overview of permanent-magnet brushless drives for electric and hybrid electric vehicles," *IEEE Trans. Ind. Electron.*, vol. 55, no. 6, pp. 2246–2257, Jun. 2008.

[2] L. Wu, H. Yin, D. Wang, and Y. Fang, "On-load field prediction in SPM machines by a subdomain and magnetic circuit hybrid model," *IEEE Trans. Ind. Electron.*, early access, Sep. 25, 2019, doi: 10.1109/TIE.2019.2942561.

[3] E. Hoang, A. H. Ben-Ahmed, and J. Lucidarme, "Switching flux permanent magnet polyphased synchronous machines," in *Proc. 7th Eur. Conf. Power Electron. Appl.*, vol. 3, Sep. 1997, pp. 903–908.

[4] Y. Liao, F. Liang, and T. A. Lipo, "A novel permanent magnet motor with doubly salient structure," *IEEE Trans. Ind. Appl.*, vol. 31, no. 5, pp. 1069–1078, Sep./Oct. 1995.

[5] R. P. Deodhar, S. Andersson, I. Boldea, and T. J. E. Miller, "The flux-reversal machine: A new brushless doubly-salient permanent-magnet machine," *IEEE Trans. Ind. Appl.*, vol. 33, no. 4, pp. 925–934, Jul./Aug. 1997.

[6] L. Zhang, L. J. Wu, X. Huang, Y. Fang, and Q. Lu, "A novel structure of doubly salient permanent magnet machine in square envelope," *IEEE Trans. Magn.*, vol. 55, no. 6, Jun. 2019, Art. no. 8103505.

[7] Z. Q. Zhu, Z. Z. Wu, D. J. Evans, and W. Q. Chu, "Novel electrical machines having separate PM excitation stator," *IEEE Trans. Magn.*, vol. 51, no. 4, Apr. 2015, Art. no. 8104109.

[8] W. Hua, H. Zhang, M. Cheng, J. Meng, and C. Hou, "An outer-rotor flux-switching permanent-magnet-machine with wedge-shaped magnets for in-wheel light traction," *IEEE Trans. Ind. Electron.*, vol. 64, no. 1, pp. 69–80, Jan. 2017.

[9] M. Cheng, W. Hua, J. Zhang, and W. Zhao, "Overview of stator-permanent magnet brushless machines," *IEEE Trans. Ind. Electron.*, vol. 58, no. 11, pp. 5087–5101, Nov. 2011.

[10] J. T. Chen and Z. Q. Zhu, "Comparison of all- and alternate-poles-wound flux-switching PM machines having different stator and rotor pole numbers," *IEEE Trans. Ind. Appl.*, vol. 46, no. 4, pp. 1406–1415, Jul./Aug. 2010.

[11] J. T. Chen, Z. Q. Zhu, S. Iwasaki, and R. P. Deodhar, "A novel E-Core switched-flux PM brushless AC machine," *IEEE Trans. Ind. Appl.*, vol. 47, no. 3, pp. 1273–1282, May 2011.

[12] J. T. Chen, Z. Q. Zhu, S. Iwasaki, and R. P. Deodhar, "Influence of slot opening on optimal stator and rotor pole combination and electromagnetic performance of switched-flux PM brushless AC machines," *IEEE Trans. Ind. Appl.*, vol. 47, no. 4, pp. 1681–1691, Jul./Aug. 2011.

[13] J. T. Chen, Z. Q. Zhu, and D. Howe, "Stator and rotor pole combinations for multi-tooth flux-switching permanent-magnet brushless AC machines," *IEEE Trans. Magn.*, vol. 44, no. 12, pp. 4659–4667, Dec. 2008.

[14] I. Boldea, L. Nicolae Tutelea, W. Xu, and M. Pucci, "Linear electric machines, drives, and MAGLEVs: An overview," *IEEE Trans. Ind. Electron.*, vol. 65, no. 9, pp. 7504–7515, Sep. 2018.

[15] R. Cao, Y. Jin, M. Lu, and Z. Zhang, "Quantitative comparison of linear flux-switching permanent magnet motor with linear induction motor for electromagnetic launch system," *IEEE Trans. Ind. Electron.*, vol. 65, no. 9, pp. 7569–7578, Sep. 2018.

[16] R. Cao, M. Lu, N. Jiang, and M. Cheng, "Comparison between linear induction motor and linear flux-switching permanent-magnet motor for railway transportation," *IEEE Trans. Ind. Electron.*, vol. 66, no. 12, pp. 9394–9405, Dec. 2019.

[17] Z. Q. Zhu, X. Chen, J. T. Chen, D. Howe, and J. S. Dai, "Novel linear flux-switching permanent magnet machines," in *Proc. Int. Conf. Electr. Mach. Syst.*, Wuhan, China, Oct. 2008, pp. 2948–2953.

[18] Y. X. Li, Q. F. Lu, J. T. Chen, and Z. Q. Zhu, "Research on combinations of primary and secondary pole numbers for linear switched-flux PM machines with odd pole number of primary," *Appl. Mech. Mater.*, vols. 416–417, pp. 401–407, Sep. 2013.

[19] W. Min, J. T. Chen, Z. Q. Zhu, Y. Zhu, M. Zhang, and G. H. Duan, "Optimization and comparison of novel E-core and C-core linear switched flux PM machines," *IEEE Trans. Magn.*, vol. 47, no. 8, pp. 2134–2141, Aug. 2011.

[20] J. Cai, Q. Lu, X. Huang, Y. Ye, and Y. Fang, "Performance investigation of a novel multi-tooth switched-flux linear motor," in *Proc. 10th Int. Conf. Ecol. Vehicles Renew. Energies (EVER)*, Monte Carlo, Monaco, Mar. 2015, pp. 1–7.

[21] Y. Shen, Q. Lu, H. Li, J. Cai, X. Huang, and Y. Fang, "Analysis of a novel double-sided yokeless multitooth linear switched-flux PM motor," *IEEE Trans. Ind. Electron.*, vol. 65, no. 2, pp. 1837–1845, Feb. 2018.

[22] D. J. Evans and Z. Q. Zhu, "Novel partitioned stator switched flux permanent magnet machines," *IEEE Trans. Magn.*, vol. 51, no. 1, Jan. 2015, Art. no. 8100114.

[23] Q. Lu, J. Shi, X. Huang, Y. Fang, and Y. Ye, "Performance of partitioned primary linear switched flux PM machines," in *Proc. 22nd Int. Conf. Electr. Mach. (ICEM)*, Sep. 2016, pp. 2486–2491.

[24] Q. Lu, Y. Yao, J. Shi, Y. Shen, X. Huang, and Y. Fang, "Design and performance investigation of novel linear switched flux PM machines," *IEEE Trans. Ind. Appl.*, vol. 53, no. 5, pp. 4590–4602, Sep./Oct. 2017.

[25] Z. Zeng and Q. Lu, "Investigation of novel partitioned-primary hybrid-excited flux-switching linear machines," *IEEE Trans. Ind. Electron.*, vol. 65, no. 12, pp. 9804–9813, Dec. 2018.

[26] H. Fan, K. T. Chau, C. Liu, and W. Li, "Doubly salient dual-PM linear machines for regenerative shock absorbers," *IEEE Trans. Magn.*, vol. 53, no. 11, pp. 1–5, Nov. 2017. 8204505

[27] X. Tang, T. Lin, and L. Zuo, "Design and optimization of a tubular linear electromagnetic vibration energy harvester," *IEEE/ASME Trans. Mechatronics*, vol. 19, no. 2, pp. 615–622, Apr. 2014.

[28] M.-T. Duong, Y.-D. Chun, P.-W. Han, B.-G. Park, D.-J. Bang, and J.-K. Lee, "Optimal design of a novel single-phase 8-slot 8-pole tubular electromagnetic shock absorber to harvest energy," *IEEE Trans. Ind. Electron.*, vol. 67, no. 2, pp. 1180–1190, Feb. 2020.

LIJIAN WU (Senior Member, IEEE) received the B.Eng. and M.Sc. degrees from the Hefei University of Technology, Hefei, China, in 2001 and 2004, respectively, and the Ph.D. degree from the University of Sheffield, Sheffield, U.K., in 2011, all in electrical engineering.

From 2004 to 2007, he was an Engineer with Delta Electronics (Shanghai) Company Ltd. From 2012 to 2013, he was with the Sheffield Siemens Wind Power Research Center, as a Design Engineer, focusing on wind power generators. From 2013 to 2016, he was an Advanced Engineer with Siemens Wind Power A/S, Denmark. Since 2016, he has been with Zhejiang University, where he is currently a Professor of electrical machines and control systems. His current research interest includes design and control of permanent magnet machines.

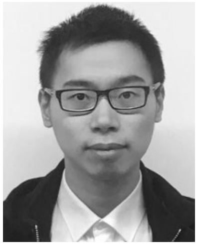

LIU ZHANG received the B.Eng. degree in electrical engineering and automation from Southwest Jiaotong University, Chengdu, China, in 2017. He is currently pursuing the Ph.D. degree with Zhejiang University, Hangzhou, China.

His research interest includes design of permanent magnet machines.

JIABEI ZHU received the B.Eng. degree in electrical engineering from Zhejiang University, Hangzhou, China, in 2017, where he is currently pursuing the Ph.D. degree.

His research interest includes design and analysis of permanent magnet machines.

QINFEN LU (Senior Member, IEEE) received the B.Eng., M.Sc., and Ph.D. degrees in electrical engineering from Zhejiang University, Hangzhou, China, in 1996, 1999, and 2005, respectively.

Since 1999, she has been with the College of Electrical Engineering, Zhejiang University, where she is currently a Professor. Her research interests include analysis and control of linear machines, and permanent-magnet machines.

YOUTONG FANG (Senior Member, IEEE) received the B.S. degree and the Ph.D. degree in electrical engineering from the Hebei University of Technology, Hebei, China, in 1984 and 2001, respectively.

He is currently a Professor with the College of Electrical Engineering, Zhejiang University, China. His research interests include the application, control, and design of electrical machines.